American Journal of Vehicle Design, 2014, Vol. 2, No. 1, 43-52
Available online at http://pubs.sciepub.com/ajvd/2/1/6
© Science and Education Publishing
DOI:10.12691/ajvd-2-1-6

Experimental Investigation and Theoretical Model Approach on Transmission Efficiency of the Vehicle Continuously Variable Transmission

Eid S. Mohamed[1,*], Saeed A. Albatlan[2]

[1]Automotive and Tractors Engineering, Faculty of Engineering, Helwan University, Mataria, Cairo, Egypt
[2]Automotive Engineering , Higher Technological institute, 10th Tenth of Ramadan city, 6th of October Branch, Cairo, Egypt
*Corresponding author: Eng_eid74@yahoo.com

Received September 09, 2014; Revised December 12, 2014; Accepted December 22, 2014

Abstract Applying a Continuously Variable Transmission (CVT) in an automotive driveline has several advantages. A CVT can operate at a wider range of transmission ratios, therefore the engine can be operated more efficiently than with a stepped transmission. The present research focuses on developing influence of loading conditions on the slip behavior and torque transmitting ability of the CVT. The aim of this work is to model of CVT investigates the range of clamping forces needed to initiate the transmission and to successfully meet the oil pressure requirements, this model has been applied on MATLAB program. An analytical approach is used the calculate possible transmission efficiency and traction coefficient of the bush belt CVT. The experimental setup and the instrumentation are present in detail; the measurement results are presented allowing for a more detailed description of the functional properties of the V-belt type variator, especially those related to reapply value of oil pressure by separate artificial hydraulic circuit and reduction ratio CVT. All the results of the practical and the theoretical investigation are presented and discussed to conclude the better operating conditions of the CVT system.

Keywords: *metal-push belt, modeling analysis of CVT, torque transmission of CVT, slip characteristics, hydraulic unit of CVT, clamping force of CVT*

Cite This Article: Eid S. Mohamed, and Saeed A. Albatlan, "Experimental Investigation and Theoretical Model Approach on Transmission Efficiency of the Vehicle Continuously Variable Transmission." *American Journal of Vehicle Design*, vol. 2, no. 1 (2014): 43-52. doi: 10.12691/ajvd-2-1-6.

1. Introduction

The CVT is increasingly used in automotive applications. It has an advantage over conventional automatic transmissions, with respect to the large transmission ratio coverage and absence of comfort issues related to shifting events. This enables the engine to operate at more economic operating points. For this reason, CVT equipped cars are more economical than cars equipped with planetary gear automatic transmissions. The key advantages of a CVT that interest vehicle manufacturers and customers can be summarized as: higher engine efficiency, higher fuel economy, smooth acceleration without shift shocks and Infinite gear ratios with a small number of parts [1].

The basic configuration of a metal V-belt CVT consists of two variable diameter pulleys connected by a power-transmitting device i.e. a metal V-belt. The pulley centers are a fixed distance apart. The pulley on the engine side is called the primary or the driver pulley. The other on the final drive (or the wheel side) is the secondary or the driven pulley. Since one of the sheaves on each pulley is movable, the application of an axial force on the movable pulley sheave allows the belt to move radially in the pulley groove. In addition to the radial motion, the belt also moves tangentially around the pulley under the influence of an applied torque. The metal V-belt is made of two series of thin steel bands holding together thin trapezoidal elements. The elements are connected to each other by a system of pegs and holes, a peg in the forward face of an element connected to a hole in the rear face of the element in front. Usually, an initial gap exists between the elements of the belt as they are not tightly pressed together [2,3].

A push-belt CVT consists of two sets of pulleys and the belt which runs inside them. The speed-ratio varies by changing the radial belt position towards the pulley center. The belt consists of two sets of bands and a large number of segments. Dynamic modelling of CVT belts have been dealt with by researchers in areas of load analysis and vibration modelling. Figure 1 illustrates the basic arrangement of a metal V-belt CVT. The band pack runs over the belt elements, whereas the belt element contacts not only the band pack, but also the pulley sheave.

In a metal V-belt continuously variable transmission (CVT), a line regular valve supplies a secondary actuator pressure while a ratio control valve generates a primary actuator pressure. The secondary actuator pressure, in other words, line pressure is required to supply a clamping force between the belt and pulley. Insufficient line

pressure causes a gross slippage of the belt, which results in a loss of power transmission capability. On the other hand, excessive line pressure causes a hydraulic loss as well as a short fatigue life of the belt. Since the line pressure can be increased up to 50 bars in the metal belt CVT, the hydraulic loss due to the high line pressure is considered to be a major powertrain loss. Therefore, in order to supply an adequate line pressure for a given driving condition, a line regulator valve which is able to provide an active control of the line pressure is required [4]. The belt-pulley friction is not constant; it depends on its operating conditions such as the angular speed, torque, and speed ratio, but it may also vary in time as it is influenced by temperature, wear of the contact surfaces, and quality of the lubrication fluid [5].

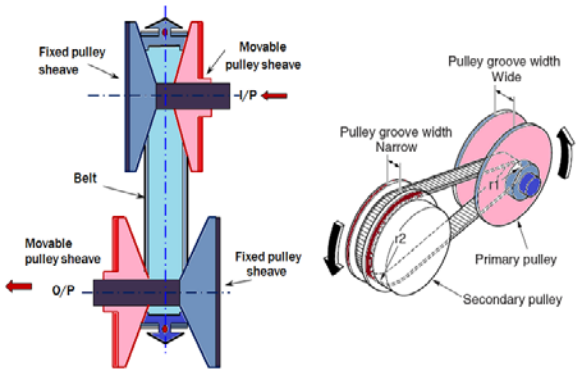

Figure 1. Pulley arrangement

[6,7] investigated the metal V-belt behavior analytically and experimentally. They proposed a speed ratio-torque load-axial force relationship to calculate belt slip. They obtained the equations of motion using quasi-static equilibrium considerations. They found that the gross slip points depend on the torque transmitting capacity of the driven side. Numerical results showed that the belt radial displacement increased in the radial inward direction for driven pulley, while that of the driver increased slightly and decreased with the increasing torque load. The effects of inertia and flexure were neglected and the band tension was assumed to be constant. Radial stiffness of belt was incorporated in order to analyze the influence of axial force on radial penetration.

[8] focused on the gap distribution between the elements and analyzed the mechanism causing microslip in a metal belt CVT. The authors also investigated the torque transmitting capacity of a metal V-belt CVT under no load conditions on driven pulley. The belt slip was calculated on the basis of mean gap (due to the redistribution of gaps among the belt elements). They showed that the slip ratio rises to a state of macroslip when the transmitted torque exceeds the slip-limit torque. The slip hypothesis made a number of assumptions: the slip was assumed to occur only on the pulley where the gaps were present and these elemental gaps were assumed to be distributed evenly in the idle sector at the entrance to the loading pulley. The metal V-belt consists of thin steel bands holding together thin trapezoidal steel elements. The elements are connected to each other by means of pegs and holes. An initial gap exists between the elements, as they are not tightly pressed together during assembly. Torque is transmitted from the driver to the driven pulley by the pushing action of the belt elements. Since there is friction between the bands and the elements, the bands, like flat belts, also aid in torque transmission. So, there is a combined push-pull action in the belt that enables torque transmission.

An accurate and fast control of the rate of change of the speed ratio is, indeed, a prerequisite to reach these goals and several researchers have been studying different solutions to optimize thecontrol strategy of the transmission and its performances [9,10].

[11,12] investigated the torque capacity of metal belt CVTs under the conditions of quasi-static equilibrium and impending slip. Moreover, since the belt was assumed to be under the conditions of gross-slip, all the frictional forces were circumferentially directed. Only the inertial effects arising from centripetal acceleration were taken into account. It was proposed that the torque transmission capacity was limited by the maximum belt tension and the associated fatigue strength of the tension members. It was observed that for a given belt design, increasing the width with proportional changes in tension capability and mass led to a proportional increase in torque capacity. Optimization with respect to belt pitch radius yielded a 1-5 % increase in the torque capacity of the CVT system. This could be larger or smaller depending on the initial configuration of the drive, the torque capacity of metal belt CVTs under the conditions of quasi-static equilibrium and impending slip. Moreover, since the belt was assumed to be under the conditions of gross-slip, all the frictional forces were circumferentially directed. Only the inertial effects arising from centripetal acceleration were taken into account. It was proposed that the torque transmission capacity was limited by the maximum belt tension and the associated fatigue strength of the tension members. It was observed that for a given belt design, increasing the width with proportional changes in tension capability and mass led to a proportional increase in torque capacity. Optimization with respect to belt pitch radius yielded a 1-5 % increase in the torque capacity of the CVT system. This could be larger or smaller depending on the initial configuration of the drive.

The influence of thermal effects on the performance and the life of a rubber V-belt drive by developing a simple heat transfer model based on conduction and convection effects. He proposed that heat is generated at the surface of the belt due to friction i.e. sliding between the belt and the pulley. Heat is also generated inside the belt due to hysteresis. The author suggested that thermal effects due to hysteresis significantly influence the life of a belt drive. And identified four major failure modes in rubber V-belts: cord rupture due to high torques, cord separation at moderate torques, radial cracks, and abrasion. Of these, cord separation mode was the most prevalent. It was attributed to the shear stresses occurring in the belt. Radial cracks start at the bottom of the belt and propagate towards the cord layer. They were attributed to the compressive stresses in the belt under low torque applications. The author also observed that abrasion was more prevalent in drives with locked-center distance than in drives with variable center distance [14].

2. Belt Geometry

The V-belt type variator appears in a few different forms. The difference is mostly the shape and materials

used in the belt or chain and the shape of the pulleys. The pulley set on the input shaft, i.e. the engine side of the transmission, is referred to as the primary pulley; the pulley set on the output shaft is called the secondary pulley. Each pulley consists of a fixed and a moveable pulley sheave [15]. The primary and secondary moveable sheaves are on opposite sides of the belt, as also shown in Figure 2 because mostly only one part of the pulley moves, the axial position of the belt is not constant

$$L = \sqrt{4C^2 - \left(d_{\sec} - d_{pri}\right)^2} + \frac{1}{2}\left(d_{pri}\beta_{pri} + d_{\sec}\beta_{\sec}\right) \quad (1)$$

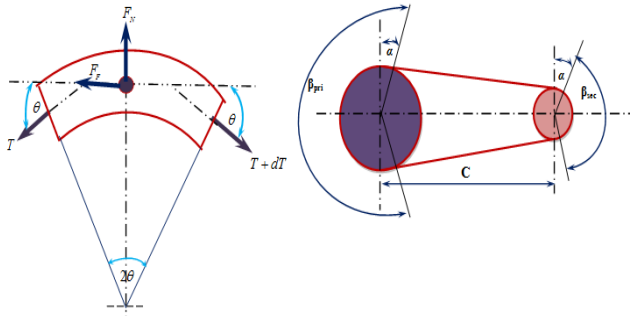

Figure 2. Geometry of the Belt

Since the length of the belt, L, is known, as is the distance between pulley centres C, the equation above can be implemented in an iterative program to find corresponding values of primary and second pulley diameters R_{pri} and R_{sec} and β_{pri} and $\beta_{\sec}$ for any value of belt ratio i. In this work the belt ratio is defined in geometric terms, as output radius over input radius, as

$$i = \frac{R_{\sec}}{R_{pri}} = \textit{Transmission ratio} \quad (2)$$

$$\begin{aligned}\beta_{pri} &= \pi - 2\sin^{-1}\left(\frac{d_{\sec} - d_{pri}}{2C}\right) \\ &= \pi - 2\sin^{-1}\left[0.5\frac{d_{\sec}}{C}(1-i)\right]\end{aligned} \quad (3)$$

$$\begin{aligned}\beta_{\sec} &= \pi + 2\sin^{-1}\left(\frac{d_{\sec} - d_{pri}}{2C}\right) \\ &= \pi + 2\sin^{-1}\left[0.5\frac{d_{\sec}}{C}(1-i)\right]\end{aligned} \quad (4)$$

3. Metal Push-belt Model

3.1. Relative Speeds between CVT Components

Consider first the relative movement between the band pack and the segments. Figure 3 shows the Relative velocities between the band pack and pulley sheave. The segments will bet travelling at a rolling radius of R_1 and R_2 about the pulleys, such that the linear speed of each of the segments; v may be calculated at loaded and no loaded as follows:

3.1.1. At no Loaded Condition

$$v = \omega_{pri}R_{pri} = \omega_{\sec}R_{\sec} \quad (5)$$

At no load spin point *(s)* is located close to center (c)
At $x=0$, $\omega_{pri}R_{pri} = \omega_{\sec}R_{\sec}$

$$\omega_{pri} = \frac{R_{\sec}}{R_{pri}}\omega_{\sec} = i\omega_{\sec} \quad (6)$$

$$v_{pri(x)} = (R_{pri} + x\sin\alpha)\omega_{pri} \Big|_{-b}^{+b}$$

and

$$v_{\sec(x)} = (R_{\sec} + x\sin\alpha)\omega_{\sec} \Big|_{-b}^{+b}$$

$$V_{s(x)} = (R_{pri} + x\sin\alpha)\omega_{pri} - (R_{\sec} + x\sin\alpha)\omega_{\sec} \Big|_{-b}^{+b} \quad (7)$$

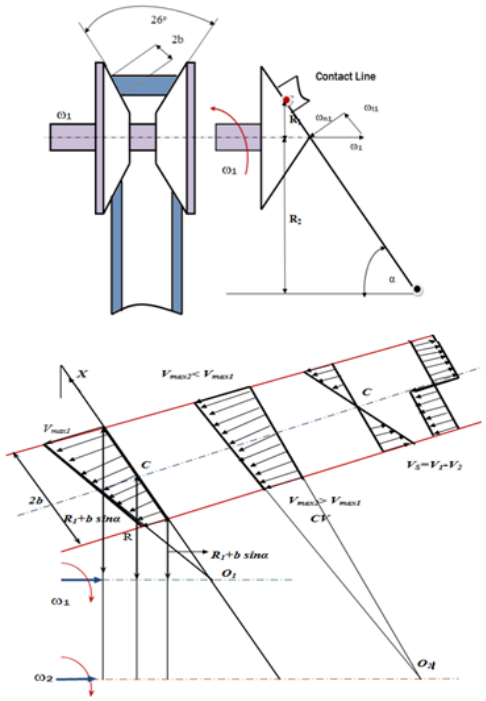

Figure 3. Relative velocities between the band pack and pulley sheave

The maximum and minimum values of velocities

$$v_{pri(\max)} = (R_{pri} + b\sin\alpha)\omega_{pri}$$

$$v_{\sec(\max)} = (R_{\sec} + b\sin\alpha)\omega_{\sec}$$

$$V_{S\max} = v_{pri(\max)} - v_{\sec(\max)} \quad (8)$$

$$V_{S\min} = v_{pri(\min)} - v_{\sec(\min)}. \quad (9)$$

3.1.2. At Loaded Conditions

The spin point moves towards the open, at the spin point; $V_s=0$ *i.e* $x=-s$

$$(R_{pri} - s\sin\alpha)\omega_{pri} = (R_{\sec} - s.\sin\alpha)\omega_{\sec}$$

$$i = \frac{\omega_{pri}}{\omega_{\sec}} = \frac{R_{\sec} - s.\sin\alpha}{R_{pri} - s.\sin\alpha} \quad (10)$$

$$V_s = \omega_{pri}\left[\begin{array}{l}(R_{pri} + x.\sin\alpha) \\ -\dfrac{(R_{\sec} + x.\sin\alpha)(R_{pri} - s.\sin\alpha)}{(R_{\sec} - s.\sin\alpha)}\end{array}\right] \quad (11)$$

3.2. Kinetics of Push Belt CVT

The CVT system runs at a steady state condition i.e. constant transmission ratio. The driver and driven pulleys run at constant angular velocities and are subjected to loading conditions of torques and axial forces. The belt inertial effects have been neglected, except for the terms arising from the centripetal acceleration of the belt. Figure 4 shows the geometry of the band pack around a number of belt segments while travelling around a pulley wrap angle. Tangential slip is modeled on the basis of gap redistribution between the belt elements. For the analysis of pushing V-belt, the following assumptions have been made [8].

$\sum F = 0$ ----------*in X-direction*

$$(T + dT)\cos\theta = F_F + T\cos\theta \quad (12)$$

$\sum F = 0$ ----------*in Y-direction*

$$(T + dT)\sin\theta + T\sin\theta = F_N \quad (13)$$

$\sum F = 0$ ----------*in tangential-direction*

$$F_T + F_P\cos\theta = (F_P + dF_P)\cos\theta + F_F \quad (14)$$

$\sum F = 0$ ----------*in radial-direction*

$$F_N + 2F_R\cos\alpha = F_C + (2F_P + dF_P)\sin\theta + 2N\sin\alpha \quad (15)$$

Where: $F_C = m\frac{v^2}{R}$

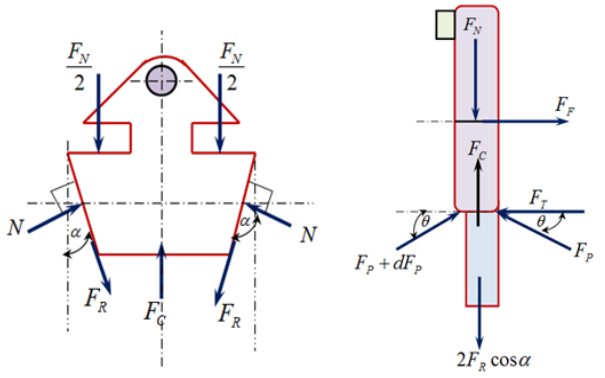

Figure 4. Free body diagram of force acting in one segment

A substitution for the normal force acting on the segment side may be made to introduce the axial force acting on the segment:

$$F_N + 2F_R = m\frac{v^2}{R} + (2F_P + dF_P)\frac{0.5t}{R} + 2F_{axle}\tan\alpha \quad (16)$$

$$F_R + F_C = (T + dT) * d\theta + T * d\theta \quad (17)$$

$$(T + dT)\cos d\theta + F_I = T\cos d\theta + F_f \quad (18)$$

3.3. Belt Friction Characteristics

The V-belt type CVT utilizes friction to transmit power from the primary pulley to the secondary pulley. The traction curve is the dimensionless relationship between transmitted torque and the slip. The maximum input torque that can be transmitted by the CVT is dependent on the applied clamping force. The belt slip speed and the belt friction coefficient increase when the transmission torque increase. The traction coefficient is therefore chosen to be a dimensionless value [16].

The traction coefficient of primary and secondary side μ_p, μ_s are defined as:

$$\mu_p = \frac{T_p\cos\alpha}{2F_pR_p} \text{ and } \mu_s = \frac{T_s\cos\alpha}{2F_sR_s} \quad (19)$$

In which T_p, T_s represent the input and output torque, R_p, R_s represent the primary and secondary running radius of the belt on the pulley, F_p , Fs represent the primary and secondary clamping forces and α is the pulley wedge angle.

The transmission efficiency of the CVT (η_T) is given by the ratio of the output and the input power of the transmission

$$\eta_T = \frac{P_{out}}{P_{inp}} = \frac{\omega_s T_s}{\omega_p T_p} \quad (20)$$

Power loss of the CVT from this equipment is

$$P_{loss} = P_{inp} - P_{out} = \frac{2\pi(n_pT_p - n_sT_s)}{60000} \quad (21)$$

The power loss given by Equation (21) includes slipping losses arising between each contacting component in the CVT, the belt torque loss caused by the resistance to radial resistance and the loss from four bearings supporting the pulley shafts.

4. Modeling Results

The simulations were conducted on MATLAB platform. The model required the input of design or configuration parameters. The characteristics of the metal belt CVT that influence its response to the loading conditions numerous simulations were done for different loading conditions in order to understand the dynamics of CVT under steady-state conditions. The impending motion in the model is such that the belt starts to move downwards in the driver pulley sheave and upwards in the driven pulley sheave. The transmission ratio for the model is defined as the ratio of belt pitch radius on driver pulley to belt pitch radius on driven pulley. Table 1 gives some of the parameter values used for simulation [17].

Table 1. The main parameters of push belt CVT

No.	Parameter	Symbol	Unit	Value
1	Pulley centre distance	C	m	0.260
2	Transmission ratio range	I_{cv}	--	2.5-0.8
3	Primary Max. input torque	T_i	N.m	120
4	Coefficient of friction	μ	---	0.15
5	Half pulley wedge angle	θ	deg.	13
6	Number of bands	i_p	---	6
7	Thickness of an individual band	t_{ban}	m	$2.1*10^{-4}$
8	Thickness of segment	t_{seg}	m	$5.5*10^{-3}$
9	Secondary spring stiffness	K_s	N/m	$10.2*10^{3}$

Figure 5 shows the calculated pulley radii about each pulley for the complete range of ratios. Using the ratio definition described above a ‘high ratio’ or ‘overdrive’ condition is described by a ratio value i_{cvt} of less than one.

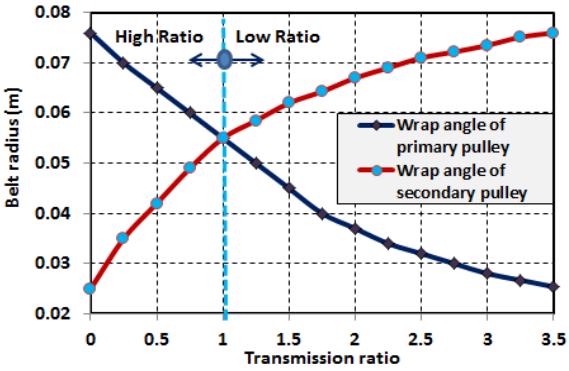

Figure 5. Belt Radii with transmission ratio

Figure 6 shows the tensile force profiles for the band pack on the driver and driven pulleys. The band tensile force decreases from the inlet to the exit of the driver pulley, whereas, it increases from the inlet to the exit of the driven pulley. Figure 7 illustrates angles of wrap about each pulley about each pulley.

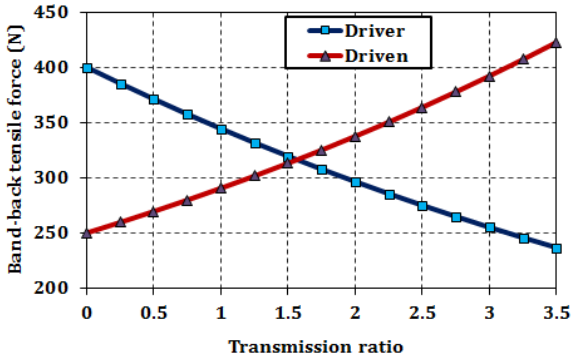

Figure 6. Variator Wrap Angles with transmission ratio

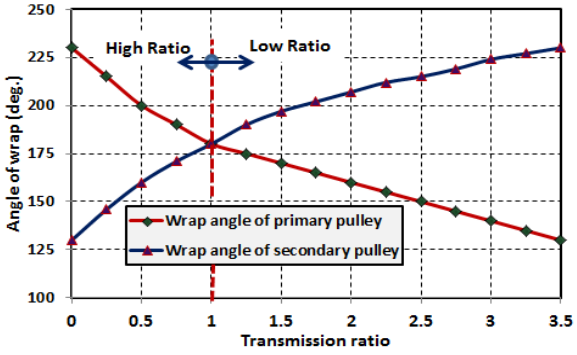

Figure 7. Band pack tensile force on the driver and driven pulleys

The simulation result with constant value of input speed 1600 rpm and torque 120 N.m, the elements pack up as the belt moves around the pulleys, and consequently the compressive force in the belt increases. Figure 8 illustrates the transmission torque with transmission ratio at different values of clamping force 1000 and 8000N at high value of axial force or clamping force to result the increase the transmission torque. Also highlights that the model is able to sustain lower load torque conditions at higher transmission ratios than at lower transmission ratios. Figure 9 and Figure 10 show the modeling results of the effective traction coefficient with different slip ratios. In Figure 9 illustrates the effective traction coefficient with primary input speed 800, 1600 and 2400 rpm conditions. And Figure 10 illustrates the effective traction coefficient with CVT transmission ratios 0.8, 1, and 2.6 conditions.

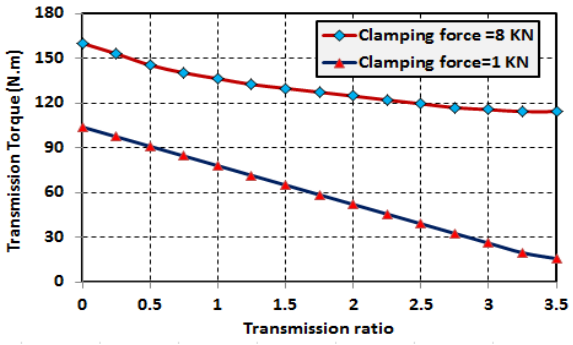

Figure 8. Transmission torque with transmission ratio

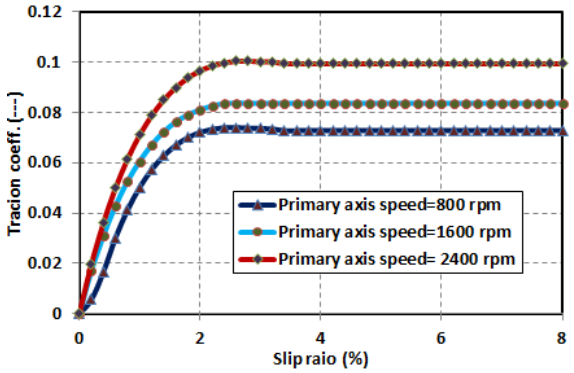

Figure 9. Traction coefficient with slip ratio at different input speed

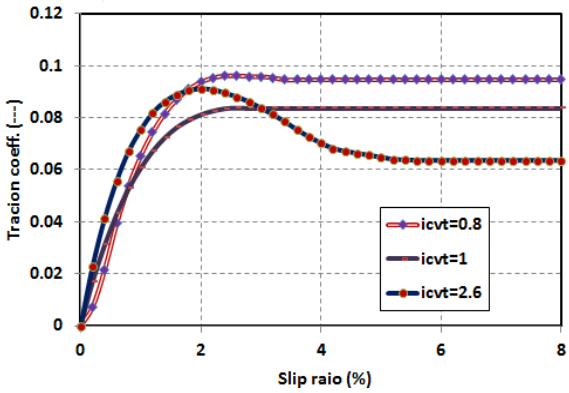

Figure 10. Traction coefficient with slip ratio at different reduction ratios

5. Experimental Work

5.1. Test Stand Setup

Figure 11 shows the test stand setup for measuring performance of the push belt CVT considered. The experimental work consists of a 25 horsepower (Hp), 3000 rev/min induction motor drawing power and driving a CVT belt system of Mitsubishi lancer GLX vehicle gearbox, a separate hydraulic brake that is couple to the output shaft of the CVT. The speed variation can be accomplished by varying the frequency to the motor with a AC inverter unit the oil pressure signals in primary and secondary line recorded were passed to the signal processing (pressre transducer, data acquisition system, laptop, and charge amplifier) with national Instruments LabVIEW™ program version 7.1 was used to create the signal recorded. The schematic diagram of the experimental set up with instrumentation details is shown in Figure 12. The motor, hydraulic disc brake, CVT

gearbox and hydraulic shift system are hard mounted and aligned on a bedplate. The bedplate is mounted using isolation feet to prevent vibration transmission to the floor. The shafts are connected with both flexible and rigid couplings.

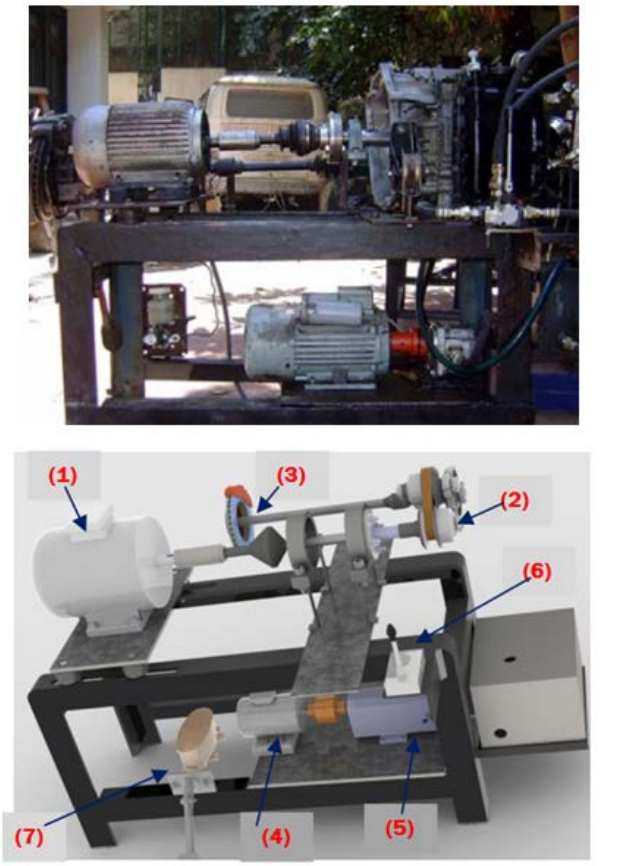

1	AC driving motor	5	Oil pressure pump
2	CVT Gearbox	6	Directional Control Valve
3	Disc brake load	7	Brake pedal and master cylinder
4	AC motor of oil pump		

Figure 11. Photograph of the layout of the test rig

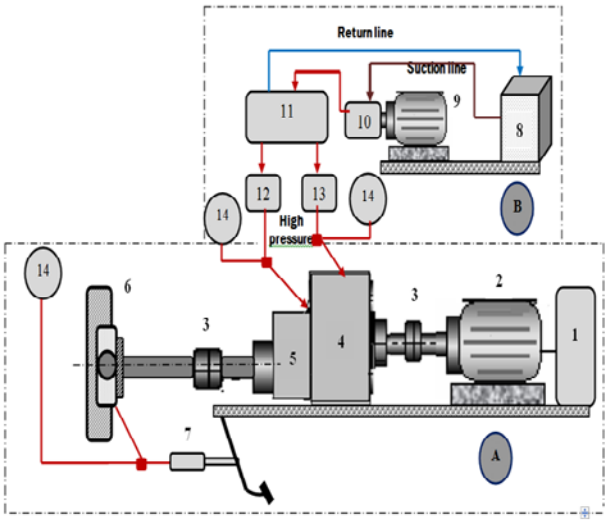

A	Mechanical Drive System	B	Hydraulic Drive System
1	3-phase inverter	8	Oil tank
2	Electrical drive motor	9	Electrical motor
3	Mechanical coupling	10	High pressure pump
4	Push belt CVT	11	Directional control valve
5	Differential final drive	12	Primary pulley choke valve
6	Brake system	13	secondary pulley choke valve
7	Brake master cylinder	14	Pressure gauge

Figure 12. Overview of the test stand layout

5.2. Hydraulic Circuit and Measuring

The measurement methodology used induction (1.5HP, 1450 rev/min) motor drawing power through an electrical source and driving hydraulic pump, the hydraulic shift system characteristics are as follows in Table 2. The hydraulic part of the CVT essentially consists of a gear pump directly connected to the driving electrical motor, the Directional Control Valve (DCV), choke valves and a pressure cylinder of the moveable pulley sheaves. The volume between the pump and the chock valves including the secondary pulley cylinder is referred to as the secondary circuit, the volume directly connected to and plus the primary pulley cylinder is the primary circuit. Excessive flow in the secondary circuit bleeds off towards the accessories, whereas the primary circuit can blow off towards the drain. Pressures are defined relative to the atmospheric drain pressure p_T. The Directional Control Valve (DCV) directs the pressurized fluid to either primary or secondary pulley as set to position A or B. In neutral position the DCV returns the fluid to the tank. The Choke Valves (CV), the throttle choke valve allows the pressure flow normally in the forward direction, and restricts (choke) the flow in the return direction. It is used here to maintain the pressure level in the pulley after shifting the pressure direction to the other pulley, the connection and operation of hydraulic shift system shows in Figure 13. As the model will only be used to determine the hydraulic system constraints needed for the feed forward control, the following assumptions have been made:

- The compressibility of the oil is neglected
- The oil temperature is constant and all leakage flows are negligible

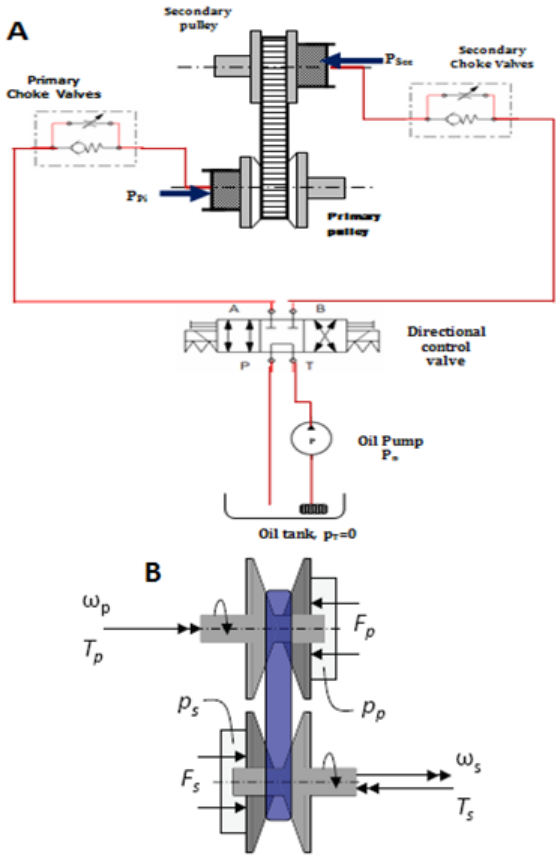

Figure 13. Schematic diagram of CVT hydraulic control circuit

Table 2. Hydraulic system characteristics

No.	Parameter	Symbols	Unit	Value
1	Drive motor power	P_m n_d	HP rpm	1.5 1420
2	Hydraulic pump flow rate	Q_p	L/min	10
4	Choke valve low rate	Q_c	L/min	15
5	Directional control valve flow rate	Q_v	L/min	30
6	Oil tank capacity	V_{oil}	Liter	1.5
7	Secondary piston diamter	A_s	cm	5
8	Primary piston area diamter	A_p	cm	10

The clamping forces F_P and F_s are realized mainly by the hydraulic cylinders on the moveable sheaves. Since the cylinders are an integral part of the pulleys, they rotate with an often very high speed, so centrifugal effects have to be taken into account and the pressure in the cylinders will not be homogeneous. Therefore, the clamping forces will also depend on the pulley speeds $\omega_{\mathrm{Pr}i}$ and ω_{Sec}. Furthermore, a prestressed linear elastic spring with stiffness K_s is attached to the moveable secondary sheave. This spring has to guarantee a minimal clamping force when the hydraulic system fails. Together this results in the following relations for the clamping forces:

$$F_p = P_P * A_p + C_p * \omega_{pri}^2 \tag{22}$$

Here, A_{p} is the primary piston area, C_p a centrifugal coefficient and P_p the oil pressure in the primary circuit.

$$F_S = P_s * A_{\mathrm{s}} + C_s * \omega_{\mathrm{sec}}^2 + K_s \Delta x + F_i \tag{23}$$

Likewise, the secondary pulley clamping force F_{s} consists of a direct pressure term $P_s * A_{\mathrm{s}}$ and a centrifugal force, with A_{s} the secondary piston surface, C_S the centrifugal coefficient and P_s the secondary pressure. Moreover, in F_{s} there is a contribution of the secondary spring F_{spr} that has to warrant a minimal clamping force under all circumstances. F_i is the force in the spring if the secondary moveable sheave is at position $\Delta x = 0$. The oil flow from the *(DCV)* to the primary circuit, by use the law of mass conservation, applied to the primary circuit:

$$Q_{DCV\to p} = C_f * A_p * x_p \sqrt{\frac{2(p_s - p_p)}{\rho}} sign(p_s - p_p) \tag{24}$$

Where C_f is a constant flow coefficient and ρ is the oil density. The equivalent valve opening area A_{sp} depends on the primary valve stem position x_{p}. The oil flow from the primary circuit to the drain

$$Q_{p\to d} = C_f * A_{pd} * x_p \sqrt{\frac{2(p_p)}{\rho}} \tag{25}$$

A_{pd} is the equivalent opening area of the primary valve for the flow from primary circuit to the drain. The oil flow from the (DCV) to the secondary circuit, by use the law of mass conservation, applied to the secondary circuit

$$Q_{DCV\to S} = C_f * A_{\mathrm{s}} * x_s \sqrt{\frac{2(p_p - p_s)}{\rho}} sign(p_p - p_s) \tag{26}$$

Application of the law of mass conservation to the hydraulic circuit yields, the flow rate of oil pump is written as:

$$Q_{pump} = Q_{DCV\to S} + Q_{DCV\to p} + Q_{p\to d} \tag{27}$$

RMS is a kind of average of pressure and clamping force signal, for discrete signals, the RMS value is defined as:

$$RMS = \sqrt{\frac{1}{N}\sum_{n=1}^{N}(x(n) - \bar{x})^2} \tag{28}$$

$$\bar{x} = \frac{1}{N}\sum_{n=1}^{N} x(n)$$

N is the number of samples taken within the signal and $x(n)$ the time domain signal and $\bar{x}$ is the mean value of all the amplitudes.

5.3. Practical Results

This section will present the results obtained from the tests carried on the push belt CVT system in the laboratory. The results will be discussed to determining the performance and response of push belt include different oil pressure and transmission ratio. A National Instruments LabVIEW™ program version 7.1 was used to create the desire software program to perform the tests required. The speed variation can be accomplished by varying the frequency to the motor with an AC inverter unit. The motor shaft speed from 800 rpm to 2400 rpm; and the load variation values by hydraulic brake system from zero to 75 N.m. The speed and loading values as used in this study are listed in Table 3.

Table 3. CVT measuring values identity

No.	AC inverter Data	Loading values data		
	Primary speed (rpm)	Brake pedal Travel, mm	Brake Pressure, bar	Torque, Nm
1	0	0	0	0
2	800	5	3	15
3	1600	10	6	45
4	2400	15	9	75

Figure 14 and Figure 15 show the samples from the translation primary and secondary pressure responses in terms of time-domain, with different input speed 800 and 2400 rpm. Figure 16 and Figure 17 show the samples from the translation primary and secondary clamping responses in terms of time-domain. And the other results show in the section comparison of result. The maximum oil pressure acting on secondary pulley piston is 48 bars at input speed 800 rpm and decease to 45 bars at increased the input speed to 2400 rpm.

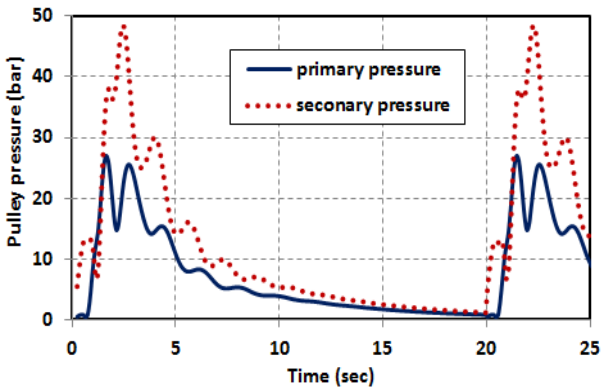

Figure 14. Translation primary and secondary pressure responses at ω_P =800rpm

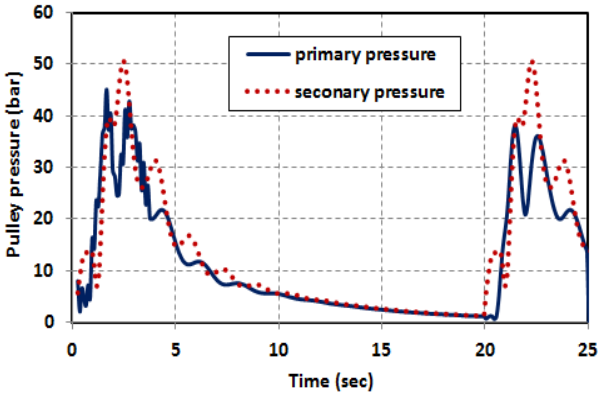

Figure 15. Translation primary and secondary pressure responses at ω_P =2400rpm

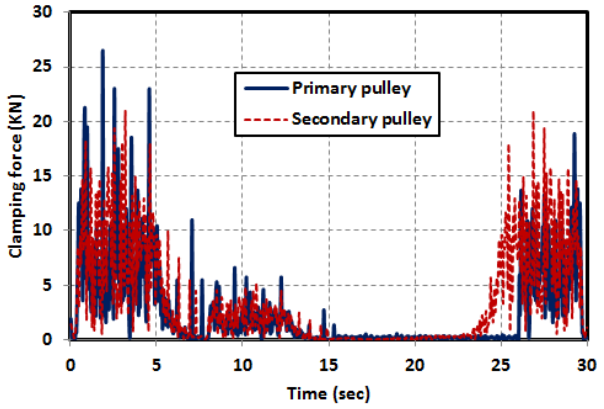

Figure 16. The clamping force responses at ω_P =800rpm

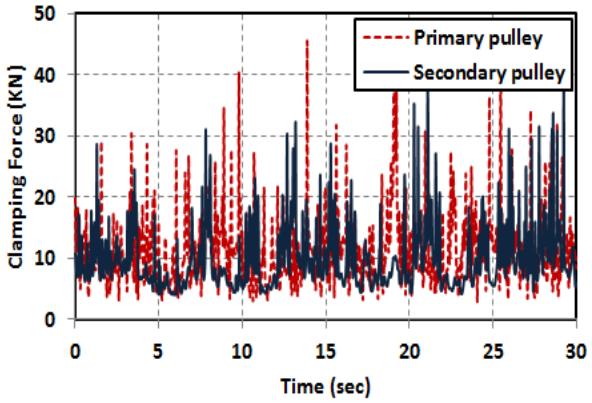

Figure 17. The clamping force responses at ω_P =2400rpm

5.4. Evaluation of Comparison Results

The comparison between theoretical and experimental results at 1600 rpm show in Figure 18 and Figure 19. In Figure 18 shows the Traction coefficient at different transmission ratio, the measured clamping force effect on the fluctuations of the traction coefficient. Figure 20 illustrates the transmission efficiency at i_{cvt}=2.6, the maximum value of efficiency equal 94% at theoretical and 90 ± 2% at experimental, the efficiency depends on oil pressure, transmission ratio and input speed. Figure 20 and Figure 21 illustrate the RMS of clamping force with different output load and different speed and i_{cvt}=2.6. Figure 22 illustrates the maximum value of transmission efficiency with different clamping force. The transmission efficient of the CVT increases with decreasing clamping force and the transmission ratio are kept constant.

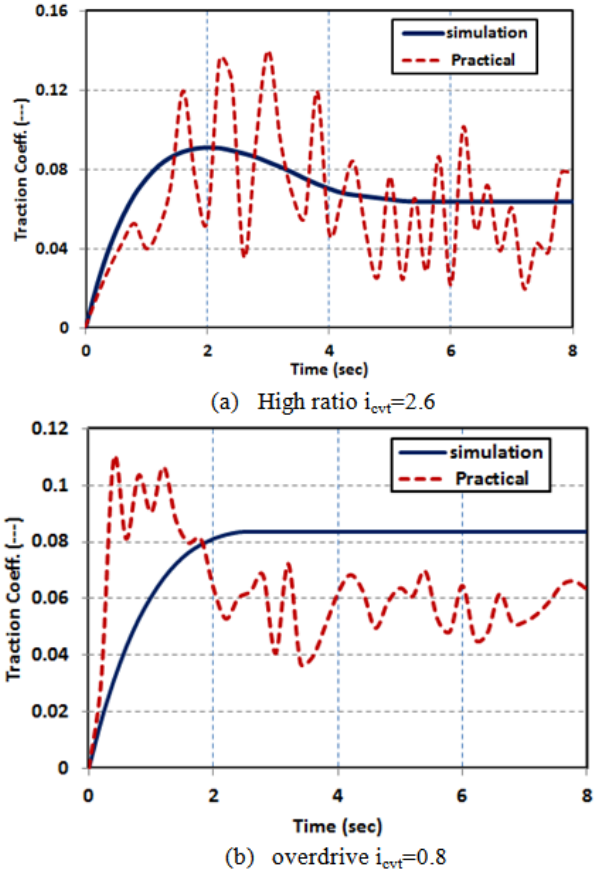

Figure 18. Comparison between simulation and practical traction coefficient =1600rpm

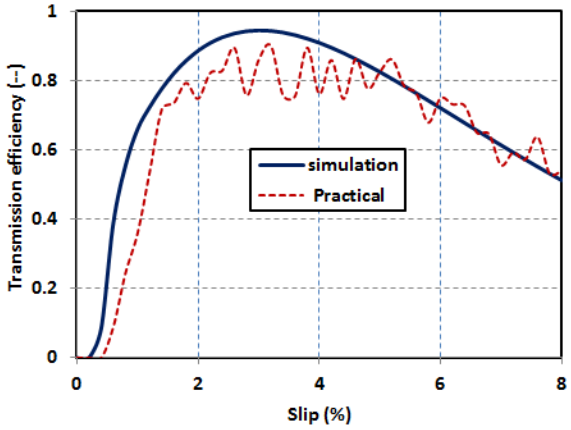

Figure 19. Comparison between simulation and practical of transmission efficiency =1600rpm

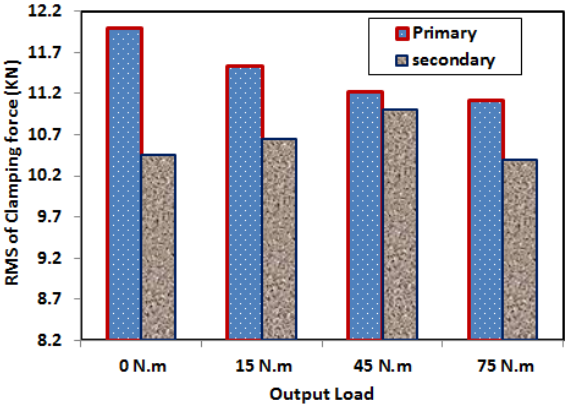

Figure 20. Comparison between simulation and practical of clamping force RMS =1600rpm

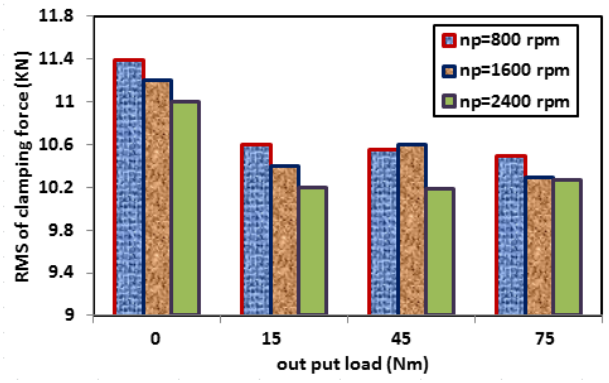

Figure 21. RMS of practical clamping force with different input speed

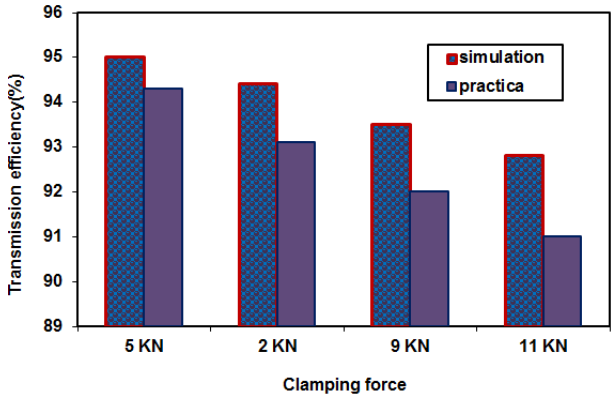

Figure 22. Comparison between simulation and practical of maximum transmission efficiency with different clamping force

6. Conclusions

In this paper, we present the dynamic analysis and experimental work with artificial clamping force of a one type of CVT. The main conclusions from the work carried out summarized in the following points:

1. Applying the different input variable parameters to the bush belt full system mathematical model which are the input speed (ω_P), the transmission ratio (i_{cvt}), the half pulley wedge angle (θ), and the slip ratio, that directly affects the system transmission performance.
2. Based on the RMS of applied pressure and clamping force of CVT gearbox, the influence of changing gearbox speed and load on the RMS value is also introduced, which confirm the discussion stated above.
3. The laboratory apparatus and experimental methodology capability established in this work could be utilized for evaluating the dynamic performance of the push belt CVT.
4. The investigated the reliability of the improved model with a theoretical-experimental comparison of a belt drives variatorn in steady state conditions. Our calculations have shown a good agreement between theory and experiments especially at high clamping forces values, either in predicting the thrust force ratio necessary to establish the desired transmission ratio either in evaluating the variator traction behaviour.

Nomenclature

List of Symbols

T	The band tension. (The total tension in both band packs.) (N)
F_I	Inertia Force (N)
T_1, T_2	Belt Tensions at ends of the Element (N)
F_c	Centrifugal Force (N)
F_F	Friction force acting between band pack and segment or between neigh boring bands (N)
F_N	Total normal force acting on the segment shoulder (N)
F_T	The tangential friction force acting between The pulley surface and the segment side (N)
F_R	Radial friction force acting between the pulley Surface and the segment sides (N)
F_{axle}	Axial force acting on the segment (N)
m	Mass of one belt segment (Kg)
V	The velocity of the segment (m/s)
R	The rolling radius of the belt segment (m)
R_{sec}	Radius of the secondary pulley (m)
R_{pr}	Radius of the primary pulley (m)
C	Center distance (m)
β_{pri}	Contact angle for primary pulley (deg.)
$\beta_{\sec}$	Contact angle for secondary pulley (deg.)
i_{cvt}	Transmission ratio of CVT (--)
L	Belt Length (m)
P_p, P_s	Primary and secondary oil pressure (N/m^2)
F_s, F_p	Secondary and primary clamping force (N)
A_p, A_s	Primary and secondary pistons area (m^2)
ω_P , ω_S	Primary and secondary pulley velocities (rpm)
x_p, x_s	Distance of the primary and secondary pistons (m)
Δx	Initial distance of secondary pulley spring (m)
F_{spr}	Force of secondary pulley spring (N)
C_p, C_s	Primary and secondary pulleys centrifugal coefficient (--)
μ_p, μ_s	Primary and secondary pulley and belt traction coefficient (--)

List of acronyms:

DCV	Directional Control Valve
CVT	Continuously Variable Transmission
CV	Choke Valves
RMS	Root Mean Square.

References

[1] Lingyuan Kong, Robert and G. Parker "Steady mechanics of layered, multi-band belt drive used in continuously variable transmissions (CVT)"science direct Mechanism and Machine Theory 43 (2008) 171-185.

[2] Shinya k., Toru fujii, and shigera K. "Study on a Metal pushing V-belt Type CVT: Band Tension and Load Distribution in Steel rings" ElSEVIER, March 1999, JSAE 20 (1999).

[3] G. Carbone,L. Mangialardi, and G. Mantriota (2002) “Influence of Clearance Between Plates in Metal Pushing V-Belt Dynamics” ASM, Journal of Mechanical Design, 2002, Vol. 124.

[4] A. Shafie, and M. H. Ali “Development of an Efficient CVT using Electromechanically System” World Academy of Science, Engineering and Technology 56, 2009, Vol. 3 2009-08-20.

[5] Arnijima, S., Fujii, T., Matsuoka, H., and Ikeda, E., 1992, ‘‘Study on Axial Force and its Distribution of a New CVT Belt for Car,’’ Int. J. Vehicle Desine, 13(2), pp. 168-181.

[6] Keunsoo J, Heera L, Talcheol Kim Jaeshin Y. and Heebock C. (2000) “Dynamic Characteristics of CVT Electro-Hydraulic Control Valves Including Shift Dynamics” Seoul 2000 FISITA World Automotive Congress, F2000A132 June 12-15, 2000, Seoul, Korea.

[7] Mohan Gangadurl, N. Harikrishnan and b. sreekumar (2005)” Development of an Analytical Design Concept of Mechanical Controlled continuously Variable Transmission” SAE Publication, 2005-26-069.

[8] B. Bonsen, T. Klaassen, and K. de Meerakker (2006)” Modeling Slip- and Creep-mode Shift Speed Characteristics of a Push-belt Type Continuously Variable Transmission” 04CVT-3.

[9] A. Mark and L. Robert. (2003) “A Hybrid Transmission for SAE Mini Baja Vehicles”. SAE Publication 2003-32-0045./20034345.

[10] Michil P., B. Vroement, Bart S., Frans V. and Maarten S. (2006)“Control of a hydraulically actuated continuously variable transmission” Vehicle System Dynamics Vol. 44, No. 5, May 2006, 387-406.

[11] Shimizu H., Kobayashi D., Kawashima J., and Kato Y., “Development of 3-D Simulation for Analyzing the Dynamic Behavior of a Metal Pushing V-Belt for CVTs”, SAE Paper, 2000-01-0828, SAE special publication (SP-1522), transmission and driveline synposium 2000, pp. 31-36.

[12] M. Kurosawa, M. Kobayashi and M. Tominaga “Development of a High Torque Capacity Belt Derive CVT with a Torque Converter” ElSEVIER, July 1998, JSAE 20(1999)281-287.

[13] Bert Pennings, Mark van D., Arjen B., Erik van G. and Marlène L. “Van Doorne CVT Fluid Test: A Test Method on Belt-Pulley Level to Select Fluids for Push Belt CVT. Applications” 2003 SAE International P.N 2003-01-3253.

[14] Christopher Ryan Willis “A Kinematic Analysis and Design of a Continuously Variable Transmission” Master of Science in Mechanical Engineering, 19 January 2006.

[15] Nilabh Srivastava (2006)” Modeling and Simulation of Friction Limited Continuously Transmission” Ph.D of Mechanical Engineering, the Graduate School of Clemson University.

[16] Eid S. Mohamed (2013) “Design and performance analysis of the hybrid powertrain strategies for split hybrid vehicles with CVT” Int. J. Electric and Hybrid Vehicles, Vol. 5, No. 3, PP. 195-214.

[17] Mangialardi, L., and Mantriota, G., (1992) “Continuously Variable Transmission with Torque-Sensing Regulators in Waterpumping Windmills,” Renewable Energy, 7(2), pp. 807-823, 1992.